DOI: 10.1002/ejic.200600725

Dinuclear and Polynuclear Bridged Azido–Nickel(II) Complexes: Synthesis, Structure Determination, and Magnetic Properties

Salah S. Massoud,*[a] Franz A. Mautner,[b] Ramon Vicente,[c] August A. Gallo,[a] and Elodie Ducasse[a]

Keywords: Nickel / Azido bridges / Crystal structure / Magnetic properties

Azido–Ni^{II} complexes of dinuclear, $[Ni_2(trpn)_2(\mu_{1,3}\text{-}N_3)_2](ClO_4)_2$ (**1**), and monodimensional structures *cis*-$[Ni(abap)(\mu_{1,3}\text{-}N_3)]_n(ClO_4)_n$ (**2**) and *cis*-$[Ni(Me_6trien)(\mu_{1,3}\text{-}N_3)]_n(ClO_4)_n \cdot nH_2O$ (**3a**) as well as the monomer $[Ni(Me_6trien)(N_3)]ClO_4$ (**3b**) {trpn = tris(3-aminopropyl)amine; abap = *N*-(2-aminoethyl)-*N*,*N*-bis(3-aminopropyl)amine; Me_6trien = 1,1,4,7,10,10-hexamethyltriethylene tetramine} were synthesized and structurally characterized by spectroscopic techniques, X-ray crystallography, and variable-temperature magnetic measurements. In the complexes **1**–**3a**, the ClO_4^- groups are counterions and the Ni^{2+} centers are bridged by the azido ligands in an end-to-end bonding fashion. The coordination geometry around the Ni^{II} ions is six-coordinate with a distorted octahedral environment achieved by the four N atoms of the tetradentate amines and two terminal N atoms of the azide groups. Complex **1** consists of dinuclear units with doubly bridged azido groups whereas in **2** and **3a**, a polymeric 1D chain is formed in which the adjacent azido groups link the Ni^{II} centers in a *cis* arrangement. In complex **2**, the structural parameters of the two adjacent azido bridging ligands are different and an alternating 1D system with two different end-to-end azido bridges is produced. Complex **3a** is a uniform 1D system where the strong steric hindrance imposed by the methyl groups of the Me_6trien ligand [diagonal N(azide)–Ni–N(amine) bond angles] causes pronounced deviation from the ideal octahedral geometry. Complex **3b** exhibits a distorted square pyramidal geometry. The complexes **1**–**3a** show antiferromagnetic coupling. In complex **1**, the exchange coupling constant was $J = -64(1)$ cm^{-1}, whereas in the polynuclear species **2** and **3a**, the calculated values were $J_1 = -63.7(2)$ ($\alpha = 0.52$) and $J = -26.8(1)$ cm^{-1}, respectively. The magnetic parameters have been correlated to the structural data.

Introduction

The pseudohalides and especially the azido bridging ligands have been reported to be efficient transmitters for propagating magnetic interaction between paramagnetic divalent metal centers (Mn^{2+}, Co^{2+}, Cu^{2+}, Ni^{2+})[1] This property makes the metal complexes derived from these ligands an attractive topic for materials scientists and for physicists,[2] and for the same reason this class of compounds was considered to be one of the most extensively studied systems in the last three decades.[3–28] This was attributed to the distinct possibilities of magnetic coupling interactions through the azide bridge and the versatility of the ligand when it binds metal ions.[4–28] In general, two different coordination modes were established in the azido/M^{2+} systems: end-to-end coordination ($\mu_{1,3}$-N_3) and end-on coordination ($\mu_{1,1}$-N_3).[4–24] Restricting our discussion to azido Ni^{II} complexes derived from amines and/or amine derivatives as blocking ligands, the azido ligand generates a variety of bonding modes ranging from discrete molecules,[4–6] dinuclear (μ_2-1,3-N_3 and μ_2-1,1-N_3)[7–18] and even polynuclear species (μ_3-1,1,1-N_3, μ_3-1,1,3-N_3, μ_4-1,1,1,1-N_3 and μ_4-1,1,3,3-N_3)[19–21] to polymeric molecules with different dimensionality ranging from 1D[22–26] to 2D[27] networks. Moreover, many 1D polymers containing alternate chains with the same or two different bonding modes (end-to-end: $\mu_{1,3}$-N_3 and end-on: $\mu_{1,1}$-N_3) were also reported.[1,26] Azido compounds with 3D network structures were separated out and characterized in the case of Mn^{II} systems.[28] The different modes of coordination of the azide group to Ni^{2+} are illustrated in Scheme 1.

In general, the end-to-end coordination mode results in antiferromagnetically coupled compounds,[1,8–13] whereas the end-on coordination gives ferromagnetically coupled compounds.[1,14,16,17] However, deviation may exist in certain cases for example in the single end-to-end bridged azido 1D compound $[Ni(5\text{-methylpyrazole})_4(\mu_{1,3}\text{-}N_3)]_n(ClO_4)_n$ ferromagnetic coupling with an exchange coupling constant $J = 6.5$ cm^{-1} was reported.[15] In alternating 1D

[a] Department of Chemistry, University of Louisiana at Lafayette, P. O. Box 44370, Lafayette, LA 70504-4370, USA
Fax: +1-337-482-5676
E-mail: ssmassoud@louisiana.edu
[b] Institut für Physikalische and Theoretische Chemie, Technische Universität Graz,
8010 Graz, Austria
E-mail: mautner@ ptc.tu-graz.ac.at
[c] Departament de Química Inorgànica, Universitat de Barcelona, Diagonal 647, 08028 Barcelona, Spain
E-mail: ramon.vicente@qi.ub.es

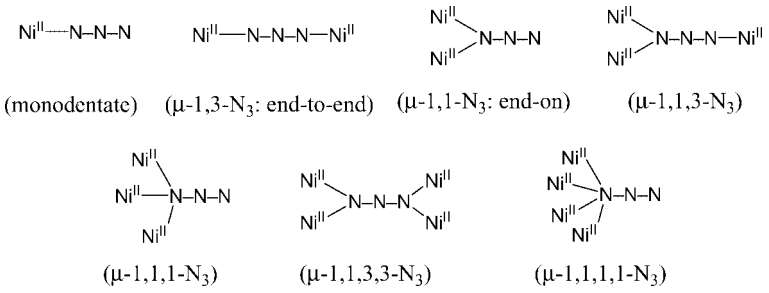

Scheme 1.

systems containing double azido bridging ligands in end-to-end and end-on coordination alternatively, two *J* values were obtained; ferromagnetic coupling with a positive *J* value corresponding to end-on azido bridging and an antiferromagnetic coupling with a negative *J* value for the end-to-end coordination.[1,26] Moreover there exists also alternating 1D systems containing single azido bridging ligands in the same end-to-end coordination mode due to the alternation in the structural parameters associated with the bridging azido environment.[1] A number of factors were addressed to correlate the magnetic behavior of the metal–azido complexes to their structural parameters. These include the intradimer M···M and M···N(azido) distances and, in the end-to-end coordination mode, the M–N–N(azido) angle and the dihedral angle, τ (the angle between the mean planes M–N1–N2–N3 and N1′–N2′–N3′–M′), in the singly bridged azido complexes or the dihedral angle, δ (the angle between the plane defined by the six *N*-azido atoms and the N1–M–N3′ plane), in the doubly bridged complexes, and also the M–(N_3)–M angle in the end-on bonding mode.[1]

The 1D *trans*-Ni($\mu_{1,3}$-N_3) systems containing one azido bridging ligand between the two nickel atoms have been widely studied from the point of view of the magnetostructural correlations.[1] However, a few studies have been reported on the corresponding *cis*-Ni($\mu_{1,3}$-N_3) systems.[1] Therefore, in an effort to shed light on the 1D *cis*-Ni($\mu_{1,3}$-N_3) systems, we have selected the tripod tetradentate amines tris(3-aminopropyl)amine (trpn), *N*-(2-aminoethyl)-*N*,*N*-bis(3-aminopropyl)amine (abap), and the sterically hindered linear tetradentate amine 1,1,4,7,10,10-hexamethyltriethylenetetramine (Me_6trien) as blocking ligands to enforce the formation of complexes of *cis*-Ni($\mu_{1,3}$-N_3) geometry. With abap and Me_6trien amines, the reactions afforded the desired 1D compounds *cis*-[Ni(abap)($\mu_{1,3}$-N_3)]$_n$(ClO_4)$_n$ (**2**) and *cis*-[Ni(Me_6trien)($\mu_{1,3}$-N_3)]$_n$(ClO_4)$_n$·*n*H_2O (**3a**), but with the trpn ligand, the dinuclear compound [Ni_2(trpn)$_2$($\mu_{1,3}$-N_3)$_2$](ClO_4)$_2$ (**1**) was produced. The magnetic properties of these complexes were measured and correlated to their structural parameters.

Results and Discussion

Synthesis and IR Spectra

The blue azido bridged dinuclear complexes [Ni_2(trpn)$_2$($\mu_{1,3}$-N_3)$_2$](ClO_4)$_2$ (**1**), and the 1D polymeric chain *cis*-[Ni(abap)($\mu_{1,3}$-N_3)]$_n$(ClO_4)$_n$ (**2**), and the anhydrous green complex [Ni(Me_6trien)(N_3)]ClO_4 (**3b**) were prepared in a reasonably good yield (74–81%) by dropwise addition of NaN_3 dissolved in H_2O to a hot aqueous solution containing equimolar amounts of Ni(ClO_4)$_2$·6H_2O and the polyamine ligand. Crystals suitable for X-ray analysis were obtained by slow evaporation of dilute aqueous solutions of the complexes at room temperature or in the refrigerator. However, it should be noted that a solid sample of the monomer [Ni(Me_6trien)(N_3)]ClO_4 (**3b**) slowly absorbs water at ambient temperature to form the polymeric species [Ni(Me_6trien)($\mu_{1,3}$-N_3)]$_n$(ClO_4)$_n$·*n*H_2O (**3a**) without losing its crystallinity (see the X-ray section). The synthesized complexes were characterized by elemental analysis and IR and UV/Vis spectroscopy.

The IR spectra of the two bridged azido complexes **1** and **2** displayed a single very strong absorption band over the range 2075–2094 cm^{-1}, whereas the fresh anhydrous [Ni(Me_6trien)(N_3)]ClO_4 revealed the band at a relatively lower frequency, 2060 cm^{-1}. The strong absorption observed in this region is attributable to the asymmetric stretching of the coordinated azido group, $\nu(N_3^-)$. The strong stretching absorption of ν(Cl–O) assigned to the noncoordinated ClO_4^- group was observed over the 1082–1092 cm^{-1} region. Interestingly, the IR spectrum of the **3b** sample which was used for the X-ray analysis and was measured after about two months of the synthesis displayed a new broad band of medium intensity centered at 3449 cm^{-1} due to the ν(O–H) of lattice water. Moreover, the azido band which was located at 2060 cm^{-1} in the parent complex disappeared, two strong bands at 2125 and 2092 cm^{-1} were detected instead, and the strong ν(Cl–O) of the perchlorate ion was slightly shifted from 1082 to 1090 cm^{-1}. On the basis of these data and the X-ray structural determination (see next section), the formula [Ni(M_6trien)($\mu_{1,3}$-N_3)]$_n$(ClO_4)$_n$·*n*H_2O (**3a**) was proposed.

Description of the Structures

[Ni(trpn)(μ$_{1,3}$-N$_3$)]$_2$(ClO$_4$)$_2$ (1)

A labeled ORTEP plot for compound **1** is shown in Figure 1 and selected bond parameters are given in Table 1. The structure of the compound consists of centrosymmetric [$C_{18}H_{48}N_{14}Ni_2$]$^{2+}$ dinuclear units in which the nickel atoms are bridged by two azide ions in a μ_2-1,3 end-to-end (EE)

fashion and ClO_4^- counterions. Each nickel atom has distorted octahedral coordination geometry. The octahedron around the Ni^{2+} center is achieved by the four N atoms of the tetradentate amine, trpn, and the two terminal N atoms of the azide groups. The Ni–N(trpn) bond lengths are in the range 2.072(4)–2.162(4) Å, and the Ni–N(N_3) bond lengths are Ni(1)–N(11) = 2.180(4) and Ni(1)–N(13) = 2.169(5) Å. The largest deviation of *cisoid* and *transoid* N–Ni–N bond angles from the ideal geometry is 8.6(2)°, whereas the N(11)–Ni(1)–N(13) bond angle is 87.3(2)°. The bond lengths of the EE-bridging azide group are N(11)–N(12) = 1.182(6) and N(12)–N(13A) = 1.163(6) Å. The Ni(1)–N(11)–N(12), Ni(1)–N(13)–N(12A), and N(11)–N(12)–N(13A) bond angles in the bridge are 119.9(3), 149.3(4), and 177.5(5)°, respectively. The Ni(1)–N(11)···N(13A)–Ni(1A) torsion angle is –19.2(7)°. The six atoms of the N_3^- bridging ligands are in one plane, and the dihedral angle between this plane and the N(11)–Ni(1)–N(13) plane is 8.3(3)°; i.e. the eight-membered $Ni_2(N_3)_2$ ring adapts a flat "chair conformation". The Ni(1)···Ni(1A) intradinuclear distance is 5.4310(16) Å, and the shortest Ni(1)···Ni(1B) interdimer distance is 5.9657(17) Å. The shortest hydrogen bond of type N–H···O (Table 4) is observed between N(3) and the perchlorate oxygen atom O(1) [2 – *x*, 1 – *y*, –*z*], with a separation of 3.121(6) Å.

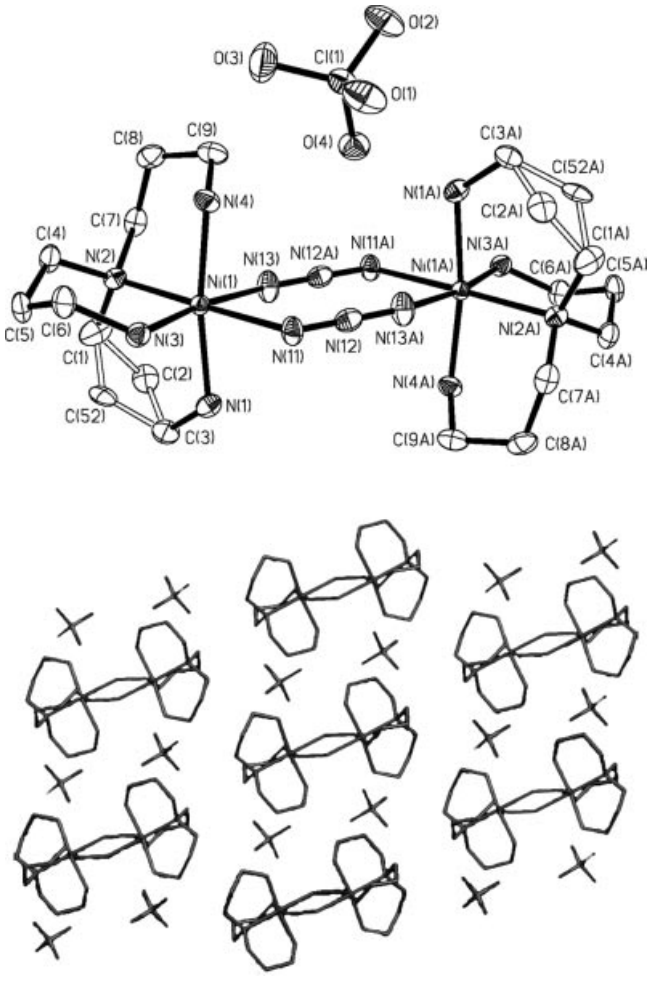

Figure 1. (top) ORTEP drawing (50% ellipsoids) and atom labeling scheme of the dinuclear complex $[Ni_2(trpn)_2(\mu_{1,3}\text{-}N_3)_2](ClO_4)_2$ (**1**). (bottom) Packing view of **1**.

Table 1. Selected bond lengths [Å] and angles [°] for $[Ni_2(trpn)_2(\mu_{1,3}\text{-}N_3)_2](ClO_4)_2$ (**1**).[a]

Ni(1)–N(3)	2.072(4)	Ni(1)–N(4)	2.085(4)
Ni(1)–N(1)	2.096(4)	Ni(1)–N(2)	2.162(4)
Ni(1)–N(13)	2.169(5)	Ni(1)–N(11)	2.180(4)
N(11)–N(12)	1.182(6)	N(12)–N(13A)	1.163(6)
Ni(1)···Ni(1A)	5.4310(16)	Ni(1)···Ni(1B)	5.9657(17)
N(3)–Ni(1)–N(4)	92.2(2)	N(3)–Ni(1)–N(1)	92.3(2)
N(4)–Ni(1)–N(1)	171.4(2)	N(3)–Ni(1)–N(2)	95.0(2)
N(4)–Ni(1)–N(2)	89.6(2)	N(1)–Ni(1)–N(2)	97.2(2)
N(3)–Ni(1)–N(13)	172.0(2)	N(4)–Ni(1)–N(13)	91.5(2)
N(1)–Ni(1)–N(13)	83.2(2)	N(2)–Ni(1)–N(13)	92.1(2)
N(3)–Ni(1)–N(11)	85.6(2)	N(4)–Ni(1)–N(11)	89.4(2)
N(1)–Ni(1)–N(11)	83.7(2)	N(2)–Ni(1)–N(11)	178.8(2)
N(13)–Ni(1)–N(11)	87.3(2)	N(12)–N(11)–Ni(1)	119.9(3)
N(13A)–N(12)–N(11)	177.5(5)	N(12A)–N(13)–Ni(1)	149.3(4)

[a] Symmetry code: (A) $-x + 2, -y, -z$; (B) $-x + 2, -y + 1, -z$.

cis-[Ni(abap)($\mu_{1,3}$-N_3)]$_n$(ClO_4)$_n$ (2)

A labeled ORTEP drawing of compound **2** is shown in Figure 2 (top) and selected bond parameters are given in Table 2. The structure of the compound consists of cationic

Table 2. Selected bond lengths [Å] and angles [°] for *cis*-[Ni(abap)($\mu_{1,3}$-N_3)]$_n$(ClO_4)$_n$ (**2**).[a]

Ni(1)–N(1)	2.099(4)	Ni(1)–N(4)	2.102(4)
Ni(1)–N(21)	2.103(4)	Ni(1)–N(3)	2.105(4)
Ni(1)–N(2)	2.131(4)	Ni(1)–N(11)	2.199(4)
N(11)–N(12)	1.181(6)	N(12)–N(13)	1.182(6)
N(13)–Ni(2)	2.178(4)	N(21)–N(22A)	1.177(5)
N(22)–N(23)	1.176(5)	N(22)–N(21B)	1.177(5)
N(23)–Ni(2)	2.109(4)	Ni(2)–N(5)	2.082(4)
Ni(2)–N(7)	2.102(4)	Ni(2)–N(8)	2.114(4)
Ni(2)–N(6)	2.135(4)	Ni(1)···Ni(2)	5.820(2)
Ni(1)···Ni(2A)	5.340(2)	Ni(1)···Ni(1B)	7.714(3)
Ni(2)···Ni(2B)	7.603(3)		
N(1)–Ni(1)–N(4)	92.7(2)	N(1)–Ni(1)–N(21)	85.3(2)
N(4)–Ni(1)–N(21)	175.5(2)	N(1)–Ni(1)–N(3)	169.6(2)
N(4)–Ni(1)–N(3)	91.3(2)	N(21)–Ni(1)–N(3)	91.4(2)
N(1)–Ni(1)–N(2)	95.1(2)	N(4)–Ni(1)–N(2)	83.6(2)
N(21)–Ni(1)–N(2)	92.5(2)	N(3)–Ni(1)–N(2)	94.9(2)
N(1)–Ni(1)–N(11)	86.8(2)	N(4)–Ni(1)–N(11)	91.1(2)
N(21)–Ni(1)–N(11)	92.8(2)	N(3)–Ni(1)–N(11)	83.6(2)
N(2)–Ni(1)–N(11)	174.5(2)	N(12)–N(11)–Ni(1)	116.0(3)
N(13)–N(12)–N(11)	179.1(5)	N(12)–N(13)–Ni(2)	117.0(3)
N(22A)–N(21)–Ni(1)	126.4(3)	N(23)–N(22)–N(21B)	177.9(5)
N(22)–N(23)–Ni(2)	131.9(3)	N(5)–Ni(2)–N(7)	169.0(2)
N(5)–Ni(2)–N(23)	85.9(2)	N(7)–Ni(2)–N(23)	92.2(2)
N(5)–Ni(2)–N(8)	91.1(2)	N(7)–Ni(2)–N(8)	91.8(2)
N(23)–Ni(2)–N(8)	173.6(2)	N(5)–Ni(2)–N(6)	96.1(2)
N(7)–Ni(2)–N(6)	94.7(2)	N(23)–Ni(2)–N(6)	91.1(2)
N(8)–Ni(2)–N(6)	83.6(2)	N(5)–Ni(2)–N(13)	85.7(2)
N(7)–Ni(2)–N(13)	83.7(2)	N(23)–Ni(2)–N(13)	93.4(2)
N(8)–Ni(2)–N(13)	92.0(2)	N(6)–Ni(2)–N(13)	175.3(2)

[a] Symmetry codes: (A) $x - 1/2, y, -z + 3/2$; (B) $x + 1/2, y, -z + 3/2$.

$[Ni(abap)(N_3)]_n^{n+}$ chains in which the nickel atoms are bridged by means of single μ_2-1,3 EE azide groups in *cis* arrangement, and ClO_4^- counterions. Within the chains two different crystallographic nickel(II) centers exist with similar distorted octahedral coordination geometry. Each NiN_6 chromophore is achieved by the four N atoms of the tetradentate abap blocking ligand, and two terminal N atoms of azide groups adopting the *cis* arrangement. The Ni–N(abap) bond lengths are in the range 2.082(4)–2.135(4) Å, and the Ni–N(N_3) bond lengths are in the range 2.103(4)–2.199(4) Å. The largest deviation of *cisoid* and *transoid* N–Ni–N bond angles from the ideal geometry is 11.0(2)°, whereas the N(11)–Ni(1)–N(21) and N(13)–Ni(2)–N(23) bond angles are 92.8(2) and 93.4(2)°, respectively. The bond lengths of the EE-bridging azide groups vary from 1.176(5) to 1.181(6) Å and the Ni–N–N bond angles from 116.0(3) to 131.9(3)°. The N(11)–N(12)–N(13) and N(23)–N(22)–N(21B) bond angles are 179.1(5) and 177.9(5)°, respectively. The Ni(1)–N(11)···N(13A)–Ni(1A) and Ni(1)–N(21)···N(23A)–Ni(2A) torsion angles are 171.0(2) and –64.3(4)°, respectively. The Ni(1)···Ni(2) and Ni(1)···Ni(2A) intrachain distances are 5.820(2) and 5.340(2) Å, whereas the shortest Ni···Ni interchain distance is 8.088(3) Å. The arrangement of the Ni–azido chain may be described as a compressed helix (Figure 2, bottom), extended along the *a* axis of the orthorhombic unit cell. Hydrogen bonds of type N–H···O and N–H···N (Table 4) form a supramolecular network.

cis-[Ni(Me$_6$trien)($\mu_{1,3}$-N$_3$)]$_n$(ClO$_4$)$_n$·nH$_2$O (3a)

An ORTEP drawing for **3a** together with the atom labeling scheme is illustrated in Figure 3 (top), and selected bond parameters are given in Table 3. The structure of **3a** consists of cationic $[Ni(Me_6trien)(N_3)]_n^{n+}$ chains in which the nickel atoms are bridged by means of single μ_2-1,3 EE azide groups in *cis* arrangement, ClO_4^- counterions, and lattice water molecules. The nickel atoms have distorted octahedral coordination geometry. Similar as in **2**, each NiN_6 chromophore is achieved by the four N atoms of the Me_6-trien ligand and two terminal N atoms of azide groups adopting *cis* arrangement. The Ni–N(Me$_6$trien) bond lengths are in the range 2.183(3)–2.234(3) Å, and the corresponding Ni–N(azide) bond lengths, Ni(1)–N(11) and Ni(1)–N(21) are 2.088(3) and 2.101(3) Å, respectively. As a

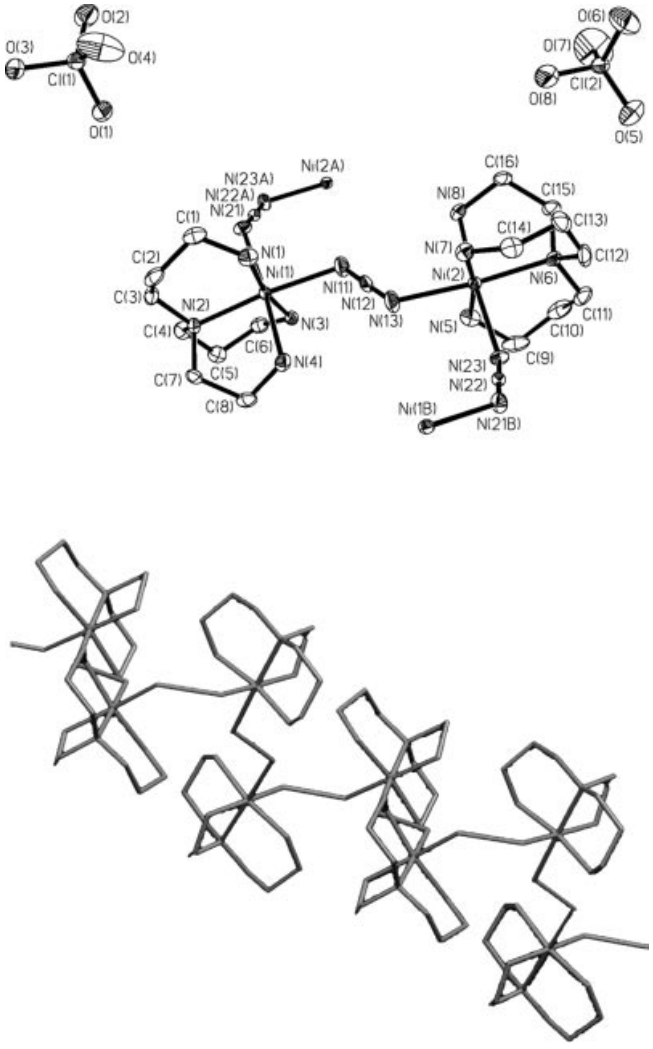

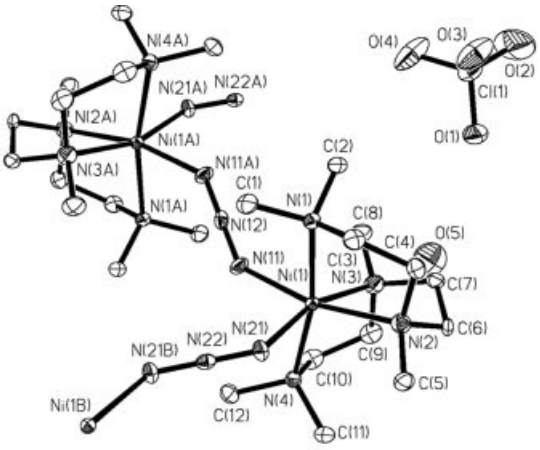

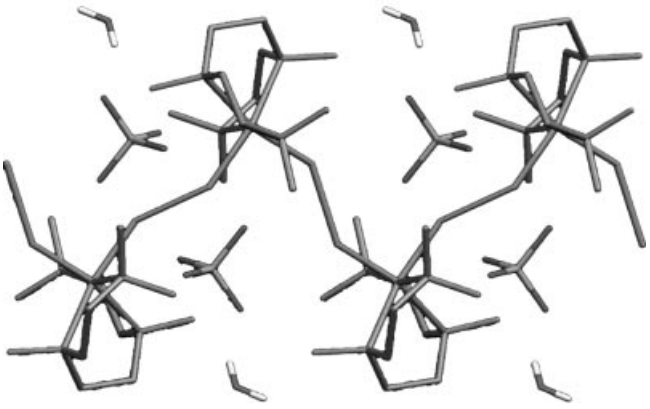

Figure 2. (top) ORTEP view (50% ellipsoids) and atom labeling scheme of *cis*-[Ni(abap)($\mu_{1,3}$-N_3)]$_n$(ClO_4)$_n$ (**2**). (bottom) The *cis*-[Ni(abap)($\mu_{1,3}$-N_3)]$_n^{n+}$ 1D chain of **2**.

Figure 3. (top) ORTEP drawing (50% ellipsoids) and atom labeling scheme of *cis*-[Ni(Me$_6$trien)($\mu_{1,3}$-N_3)]$_n$(ClO_4)$_n$·nH_2O (**3a**). (bottom) Crystal packing of **3a**.

consequence of the bulky Me_6trien blocking ligand, the N–Ni–N bond angles deviate up to 17.3(2)° from the ideal octahedral geometry, the N(11)–Ni(1)–N(21) bond angle is 96.90(13)°. The central nitrogen atoms of the two EE-bridging azide groups are located at inversion centers where the azide groups are symmetric [N(11)–N(12) = 1.174(3), N(21)–N(22) = 1.175(3) Å] and linear [N–N–N = 180°]. The Ni(1)–N(11)–N(12) and Ni(1)–N(21)–N(22) bond angles are 138.8(2) and 135.8(2)°, respectively. The Ni(1)–N(11)···N(11A)–Ni(1A) and Ni(1)–N(21)···N(21B)–Ni(1B) torsion angles both are 180°. The Ni(1)···Ni(1A) and Ni(1)···Ni(1B) intrachain distances are 6.1412(16) and 6.1110(15) Å, respectively, whereas the shortest Ni···Ni interchain distance is 8.619(2) Å. The Ni–azide "zigzag" chain extends along the *a* axis of the orthorhombic unit cell (Figure 3 bottom). Lattice water molecules form hydrogen bonds (Table 4) of the type O–H···O to oxygen atoms O(3) of perchlorate counterions [with O···O distances of 2.956(6) and 3.337(6) Å].

Table 4. Selected hydrogen bonds in $[Ni_2(trpn)_2(\mu_{1,3}\text{-}N_3)_2](ClO_4)_2$ (**1**), *cis*-$[Ni(abap)\text{-}(\mu_{1,3}\text{-}N_3)]_n(ClO_4)_n$ (**2**), and *cis*-$[Ni(Me_6trien)(\mu_{1,3}\text{-}N_3)]_n(ClO_4)_n{\cdot}nH_2O$ (**3a**).

Comp.	D–H···A[a]	D···A [Å]	DHA [°]	Symmetry code of A
1	N(1)–H(1B)···O(1)	3.155(6)	148.1	2 – *x*, 1 – *y*, –*z*
	N(3)–H(3A)···O(1)	3.121(6)	175.1	2 – *x*, 1 – *y*, –*z*
	N(3)–H(3B)···N(11)	3.166(6)	154.0	2 – *x*, 1 – *y*, –*z*
	N(4)–H(4A)···O(3)	3.289(7)	152.0	1 – *x*, 1 – *y*, –*z*
	N(4)–H(4B)···O(4)	3.142(7)	156.7	
2	N(1)–H(1A)···O(6)	3.003(6)	172.3	1 – *x*, 1/2 + *y*, 3/2 – *z*
	N(1)–H(1B)···O(4)	3.144(6)	172.7	1 – *x*, –*y*, 1 – *z*
	N(3)–H(3C)···N(13)	3.408(6)	151.9	–1/2 + *x*, *y*, 3/2 + *z*
	N(3)–H(3D)···O(8)	3.178(6)	161.2	1/2 – *x*, 1/2 + *y*, *z*
	N(4)–H(4C)···O(7)	3.267(8)	166.8	1/2 – *x*, 1/2 + *y*, *z*
	N(4)–H(4D)···O(6)	3.256(6)	163.2	1 – *x*, 1/2 + *y*, 3/2 – *z*
	N(5)–H(5C)···O(7)	2.387(8)	170.1	1/2 – *x*, 1/2 + *y*, *z*
	N(5)–H(5D)···O(2)	3.072(6)	168.2	1/2 – *x*, –*y*, 1/2 + *z*
	N(7)–H(7C)···O(3)	3.270(7)	167.7	1 – *x*, –*y*, 1 – *z*
	N(8)–H(8C)···O(2)	3.217(5)	164.9	1/2 – *x*, –*y*, 1/2 + *z*
	N(8)–H(8D)···O(3)	3.047(7)	139.7	1 – *x*, –*y*, 1 – *z*
3a	O(5)–H(51)···O(3)	3.337(6)	155.2	1/2 – *x*, –1/2 + *y*, 3/2 – *z*
	O(5)–H(52)···O(3)	2.956(6)	168.0	–1/2 + *x*, 1/2 – *y*, –1/2 + *z*

[a] D = donor, A = acceptor.

Table 3. Selected bond lengths [Å] and angles [°] for *cis*-$[Ni(Me_6trien)(\mu_{1,3}\text{-}N_3)]_n(ClO_4)_n{\cdot}nH_2O$ (**3a**).[a]

Ni(1)–N(11)	2.088(3)	Ni(1)–N(21)	2.101(3)
Ni(1)–N(2)	2.183(3)	Ni(1)–N(3)	2.193(3)
Ni(1)–N(4)	2.203(3)	Ni(1)–N(1)	2.234(3)
N(11)–N(12)	1.174(3)	N(12)–N(11A)	1.174(3)
N(21)–N(22)	1.175(3)	N(22)–N(21B)	1.175(3)
Ni(1)···Ni(1A)	6.1412(16)	Ni(1)···Ni(1B)	6.1110(15)
N(11)–Ni(1)–N(21)	96.90(13)	N(11)–Ni(1)–N(2)	166.86(13)
N(21)–Ni(1)–N(2)	90.25(12)	N(11)–Ni(1)–N(3)	94.43(13)
N(21)–Ni(1)–N(3)	162.74(13)	N(2)–Ni(1)–N(3)	81.32(13)
N(11)–Ni(1)–N(4)	84.64(12)	N(21)–Ni(1)–N(4)	86.41(12)
N(2)–Ni(1)–N(4)	106.88(12)	N(3)–Ni(1)–N(4)	81.72(13)
N(11)–Ni(1)–N(1)	87.04(13)	N(21)–Ni(1)–N(1)	86.90(12)
N(2)–Ni(1)–N(1)	82.35(12)	N(3)–Ni(1)–N(1)	106.70(12)
N(4)–Ni(1)–N(1)	168.62(12)	N(12)–N(11)–Ni(1)	138.8(2)
N(11)–N(12)–N(11A)	180.0	N(22)–N(21)–Ni(1)	135.8(2)
N(21)–N(22)–N(21B)	180.0		

[a] Symmetry codes: (A) –*x* + 1, –*y*, –*z* + 2; (B) –*x* + 2, –*y*, –*z* + 2.

[Ni(Me$_6$trien)(N$_3$)]ClO$_4$ (3b)

An ORTEP drawing for **3b** together with the atom labeling scheme is illustrated in Figure 4, and selected bond parameters are given in Table 5. The structure of **3b** consists of monomeric $[Ni(Me_6trien)(N_3)]^+$ complex cations and ClO_4^- counterions. The NiN_5 chromophore may be described as a distorted square pyramid (τ = 0.117)[29] with N(11) of the azide group, N(1), N(2), and N(3) of the Me_6-trien ligand in basal sites and N(4) or N(5) of the partially disordered tetramine ligand at the apical site. The Ni(1)–N bond lengths range from 1.997(2) to 2.135(2) Å. In contrast to the symmetric EE azide bridges in **3a**, the monodentate azido group has asymmetric bond parameters [N(1)–N(2) = 1.189(3), N(2)–N(3) = 1.159(3) Å, N(11)–N(12)–N(13) =

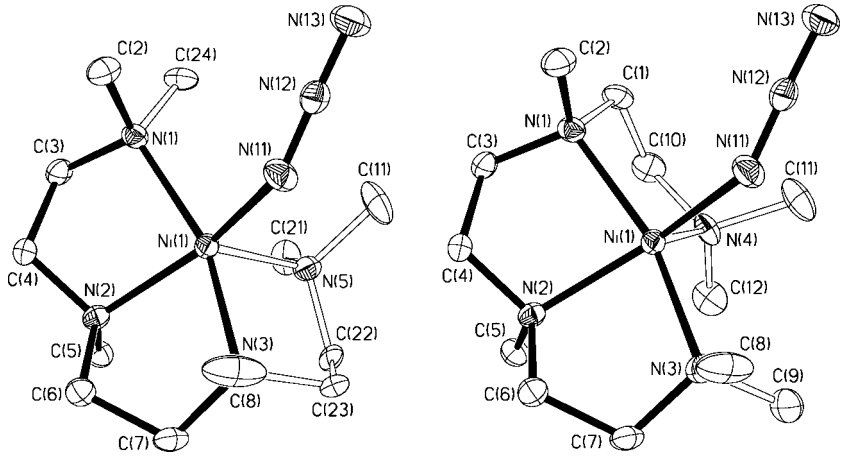

Figure 4. $[Ni(Me_6trien)(N_3)]ClO_4$ (**3b**): ORTEP drawing (50% ellipsoids) and atom labeling scheme of the two split orientations of complex cation. Open stick bonds indicate disordered parts of the Me_6trien ligand with 50% occupancy.

176.7(3)°]. The shortest Ni···Ni and N(13)···Ni distances to adjacent monomeric units are 7.584(3) and 5.403(5) Å, respectively.

Table 5. Selected bond lengths [Å] and angles [°] for [Ni(Me_6trien)(N_3)]ClO_4 (**3b**).

Ni(1)–N(11)	1.997(2)	Ni(1)–N(1)	2.122(2)
Ni(1)–N(2)	2.135(2)	Ni(1)–N(3)	2.105(3)
Ni(1)–N(4)	2.049(7)	Ni(1)–N(5)	2.119(7)
N(11)–N(12)	1.189(3)	N(12)–N(13)	1.159(3)
N(11)–Ni(1)–N(4)	99.3(2)	N(11)–Ni(1)–N(3)	89.12(10)
N(4)–Ni(1)–N(3)	108.1(2)	N(11)–Ni(1)–N(5)	98.0(2)
N(3)–Ni(1)–N(5)	89.7(2)	N(11)–Ni(1)–N(1)	95.13(10)
N(4)–Ni(1)–N(1)	90.4(2)	N(3)–Ni(1)–N(1)	160.13(10)
N(5)–Ni(1)–N(1)	108.8(2)	N(11)–Ni(1)–N(2)	153.13(10)
N(4)–Ni(1)–N(2)	107.5(2)	N(3)–Ni(1)–N(2)	83.63(10)
N(5)–Ni(1)–N(2)	107.7(2)	N(1)–Ni(1)–N(2)	83.88(9)
N(11)–N(12)–N(13)	176.7(3)	N(12)–N(11)–Ni(1)	137.8(2)

Electronic Spectra

The UV/Vis spectra of the azido–nickel(II) complexes under investigation were recorded in the solid state and in H_2O. In addition the polymer [Ni(Me_6trien)($\mu_{1,3}$-N_3)]$_n$-(ClO_4)$_n$·$n$$H_2O$ (**3a**) and its monomer (**3b**) were also measured in different organic solvents, and the data are collected in Table 6. The solid and the aqueous solution spectra of [Ni_2(trpn)$_2$($\mu_{1,3}$-N_3)$_2$]$^{2+}$ and [Ni(abap)$_2$($\mu_{1,3}$-N_3)]$_n^{n+}$ display two bands over 360–370 and 570–590 nm, and a shoulder or broad band over 770–1000 nm range. Similarly, the electronic diffuse reflectance spectrum of **3a**, [Ni(Me_6-trien)($\mu_{1,3}$-N_3)]$_n$(ClO_4)$_n$·$n$$H_2O$ reveals the presence of the three absorption bands at 367, 655, and ca. 900 nm. These spectral features are consistent with six-coordinate octahedral geometry for Ni^{II} complexes and the spectrum of the complex ions of **1**, **2**, or **3a** is adequately explained by d-d transitions in the Ni^{2+} ion in a distorted octahedral environment where the last two maxima observed in the visible region result from $^3A_{2g}$→$^3T_{1g}$(F) and $^3A_{2g}$→$^3T_{2g}$(F) transitions, respectively, and the high energy band from the $^3A_{2g}$→$^3T_{1g}$(P) transition. When the spectra of **1** were measured in organic solvents (CH_3CN, CH_3NO_2, dmso, dmf), the positions of λ_{max} did not show any significant change and were almost independent of the nature of the solvent used. The insolubility and/or the very low solubility of complex **2** prohibit measuring its spectrum in organic solvents. The reflectance spectra of the complexes **1**–**3a** showed low resolution and the fact that the low energy broad band was detected at higher wavelengths ($\lambda_{max} \geq 900$ nm) compared to that observed in H_2O or other solvent may be attributed to the contribution of the vibrational transitions in this region. Interestingly, these findings in solutions and in the solid state were consistent with the distorted octahedral geometry around the Ni^{2+} ion as determined by X-ray.

The electronic diffuse reflectance spectrum of the complex [Ni(Me_6trien)(N_3)]ClO_4 (**3b**) displays two bands at 659 nm and a shoulder at 477 nm besides a very broad band at ca. 960 nm (Table 6). Although this spectrum was not completely conclusive, it is most likely consistent with the presence of a five-coordinate environment around the Ni^{2+} center where the first two bands could be assigned to $^3B_1$ (F)→^3E (F) and $^3B_1$ (F)→$^3A_2$, ^3E (P) transitions, respectively.[30] When the spectra of the complex were measured in different coordinated solvents, the dissolution was associated with color change and the visible spectrum exhibits strong dependence on the nature of the solvent used. The spectra reveal the presence of the three bands typical for distorted octahedral Ni^{II} complexes as indicated above. The six-coordinate geometry in **3b** was achieved by the addition of a solvent molecule to the coordinatively unsaturated nickel(II) center to form [Ni(Me_6trien)(N_3)(solv)]$^+$ where the ligand field strength increases in the order: CH_3NO_2 < dmf < H_2O < CH_3CN < dmso. Similar spectral dependence was also observed for the corresponding polymer [Ni-(Me_6trien)($\mu_{1,3}$-N_3)]$_n$(ClO_4)$_n$·$n$$H_2O$ (**3a**) in CH_3CN and in dmso (Table 6) which clearly demonstrates the octahedral geometry for the central Ni^{2+} ion. The fact that in the same solvent, the monomer **3b** and the polymer **3a** gave absorption bands which are different in position and intensity might rule out the formation of the same six-coordinate species and instead a different octahedral Ni^{II} species is

Table 6. Electronic spectroscopic data for the azido–nickel(II) complexes.

Complex	Solvent	λ_{max} [nm] (ε_{max}, $M^{-1}cm^{-1}$)
[Ni_2(trpn)$_2$($\mu_{1,3}$-N_3)$_2$](ClO_4)$_2$ (**1**)	solid[a]	360 (sh), 578, 980 (br)
	H_2O	369 (49), 592 (29), 840 (5.0, br)
cis-[Ni(abap)($\mu_{1,3}$-N_3)]$_n$(ClO_4)$_n$ (**2**)	solid[a]	360 (sh), 570, 995 (br)
	H_2O/CH_3CN[b]	356 (29), 570 (18), 770 (sh)
cis-[Ni(Me_6trien)($\mu_{1,3}$-N_3)]$_n$(ClO_4)$_n$·$n$$H_2O$ (**3a**)	solid[a]	367, 655, ca. 900 (br)
	H_2O	393 (38), 662 (27), 750 (27)
	CH_3CN	ca. 390 (sh, 85), 659 (29), 745 (29)
	dmso	ca. 408 (sh, 71), 671 (28), 747 (26)
[Ni(Me_6trien)(N_3)]ClO_4 (**3b**)	solid[a]	477 (sh), 659, ca. 960 (vbr)
	H_2O[c]	394, 656, 749
	CH_3CN	392 (82), 643 (23), 737 (18)
	dmso	ca. 364 (ca. 191), 415 (75), 676 (23)
	CH_3NO_2	ca. 489 (ca. 31), 669 (39), 862 (29)
	dmf	404 (57), 656 (25), 739 (18)

[a] Reflectance spectra for solid samples were diluted with $BaSO_4$ and measured against $BaSO_4$ standard. [b] Fifty percent by volume H_2O/CH_3CN. [c] Saturated solution.

produced in solution from the polymer **3a**. Upon dissolution, the complex $[Ni(Me_6trien)(\mu_{1,3}\text{-}N_3)]_n(ClO_4)_n{\cdot}nH_2O$ undergoes solvolysis via bond rupture of the bridged Ni–N(azido) bonds and displacement of one of the azido ligands with a solvent molecule to form the dimeric six-coordinate species, $[(solv)(Me_6trien)Ni(\mu_{1,3}\text{-}N_3)Ni(Me_6trien)(solv)]^{3+}$. The interaction of the solvent molecules with $[Ni(Me_6trien)(\mu_{1,3}\text{-}N_3)]_n^{n+}$ is not surprising in terms of the strong steric hindrance imposed by the methyl groups of Me_6trien in $[Ni(Me_6trien)(\mu_{1,3}\text{-}N_3)]_n^{n+}$ where the two diagonal N(azido)–Ni–N(amine) bond angles namely N(21)–Ni(1)–N(3) and N(11)–Ni(1)–N(2) deviate from the ideal octahedral geometry by 17.3 and 13.1°, respectively. Therefore, the Ni–N(azido) bond rupture and an azide displacement with solvent molecule seems to reduce the magnitude of crowding. A similar solvent effect was also observed in the dinuclear doubly bridged end-to-end azido complex $[Cu(Et_2dien)(\mu_{1,3}\text{-}N_3)]_2(ClO_4)_2$, where Et_2dien = *N*,*N*-diethyldiethylenetriamine.[3a] However, it is difficult to propose with certainty any nuclearity for the species in solution without measuring the electrical conductivity.

Magnetic Properties

The molar magnetic susceptibility, χ_M, for polycrystalline samples of **1**, **2**, and **3a** were measured as a function of temperature and the plots of χ_M vs. T are illustrated in Figure 5, Figure 6, and Figure 7, respectively. At room temperature compound **1** exhibits a χ_M value of 7.6×10^{-3} cm^{3}mol^{-1}. This value increases as the temperature decreases, reaching a broad maximum of 14.2×10^{-3} cm^{3}mol^{-1} at ca. 70 K. Below this temperature, the molar magnetic susceptibility decreases continuously and reaches a minimum value of 6.77×10^{-3} cm^{3}mol^{-1} at 2 K. Careful inspection of the graph in Figure 5 clearly indicates a small change in the slope of the curve around 25 K which can be attributed to a little structural change. The susceptibility data in the range 25–300 K for **1** were fitted to the expression [Equation (1)] for the magnetic susceptibility of isotropically coupled S = 1 dinuclear compounds, derived from the Hamiltonian $H = -JS_1S_2$:

$$\chi_M = [0.375g^2/(T-\theta)]\{[2\exp(x) + 10\exp(3x)]/[1 + 3\exp(x) + 5\exp(3x)]\} \quad (1)$$

A Weiss θ parameter was introduced in the formula to take into consideration the possible antiferromagnetic interactions between the dinuclear molecules. The results of the best fit, shown as the solid line in Figure 5, were J = –64(1) cm^{-1}, g = 2.34(1), and θ = 14(1) K. Dinuclear complexes with core formula $[Ni_2(\mu_{1,3}\text{-}N_3)_2]^{2+}$ are known to develop a magnetostructural relationship between the exchange coupling constant, J, and the structural parameters.[1,9a] The main factor determining the $|J|$ value is the [Ni–$(\mu_{1,3}\text{-}N_3)_2$–Ni] dihedral angle, δ; the more planar the structure (δ is close to 0°) the more antiferromagnetic the interaction and hence the higher $|J|$.[1,9a] In this compound, the small dihedral angle δ (8.3°) should account for the relatively high observed $|J|$ value (64 cm^{-1}).

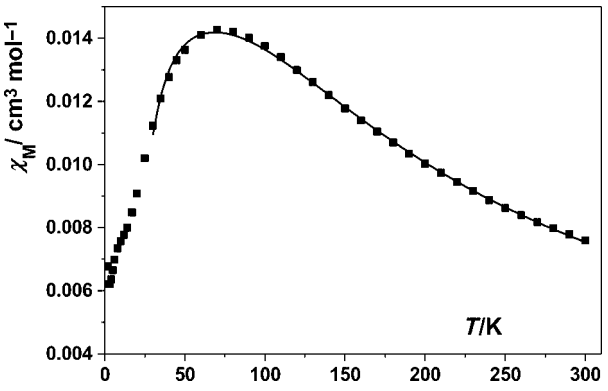

Figure 5. Plot of χ_M vs. T in the 300–2 K temperature range for $[Ni_2(trpn)_2(\mu_{1,3}\text{-}N_3)_2](ClO_4)_2$ (**1**) measured on cooling under an external magnetic field of 0.7 T. The solid line shows the best fit as a dinuclear compound (see text).

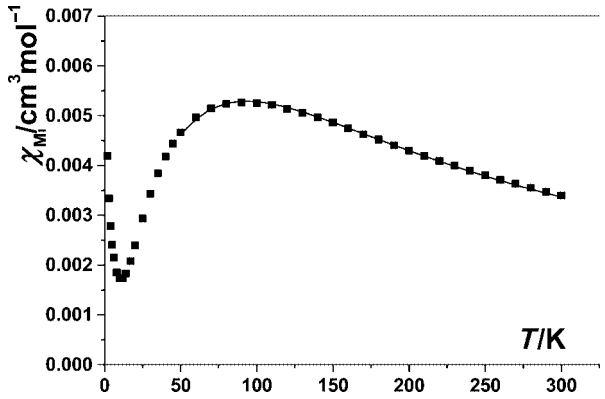

Figure 6. Plot of χ_M vs. T in the 300–2 K temperature range for *cis*-$[Ni(abap)(\mu_{1,3}\text{-}N_3)]_n(ClO_4)_n$ (**2**) measured on cooling under an external magnetic field of 0.7 T. The solid line shows the best fit as an alternating antiferromagnetic chain (see text).

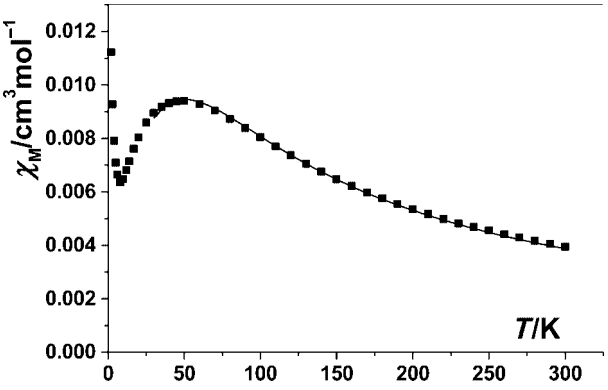

Figure 7. Plot of χ_M vs. T in the 300–2 K temperature range for *cis*-$[Ni(Me_6trien)(\mu_{1,3}\text{-}N_3)]_n(ClO_4)_n{\cdot}nH_2O$ (**3a**) measured on cooling under external magnetic field of 0.7 T. The solid line shows the best fit as a uniform antiferromagnetic chain (see text).

For compound **2**, the χ_M value at room temperature (3.48×10^{-3} cm^{3}mol^{-1}) increases as the temperature decreases, reaching a broad maximum of 5.35×10^{-3} cm^{3}mol^{-1} at ca. 90 K (Figure 6). This high temperature maximum clearly indicates strong antiferromagnetic coupling between the Ni^{II} ions through the azido brid-

ges. Below this temperature, the molar magnetic susceptibility decreases continuously and reaches a minimum value of 1.82×10^{-3} cm^3 mol^{-1} at 10 K. Beyond this temperature, χ_M increases sharply to a value of 4.28×10^{-3} cm^3 mol^{-1} at 2 K, most likely due to the presence of paramagnetic impurities.

In a first approach, experimental data were fitted up to near the maximum to the Weng equation[31] for uniform chains based on the Hamiltonian $H = -J\sum_i S_i \cdot S_{i+1}$, where the nickel ion and the exchange interaction are isotropic. The fitting is only possible up to near the maximum (in our case up to 90 K) because neither the zero-field splitting nor the Haldane gap are taken into account.[32] The best parameters so obtained were $J = -49.4(1)$ cm^{-1} and $g = 2.40(2)$. The high J value indicates a good superexchange pathway. When the alternating chain structure of compound **2** was taken into account, the coupling parameters were optimized up to 50 K by using Equation (1) for an alternating chain[33] based on the Hamiltonian $H = -J_1[\Sigma^N_{i=1} S_{2i}S_{2i+1} + \alpha\Sigma^N_{i=1} S_{2i}S_{2i-1}]$ [Equation (2)]:

$$\chi_M = (2Ng^2\mu_B^2/3kT)/(X_r T_r) \quad (2)$$

in which [Equation (3)]:

$$X_r T_r = (AT_r^2 + BT_r + C)/(T_r^3 + DT_r^2 + ET_r + F) \quad (3)$$

with $T_r = kT/|J_1|$, $X_r = 3\chi_M|J_1|/2N_A g^2\mu_B$, and $\alpha = |J_2|/|J_1|$. A–F are polynomial expressions of the α alternance parameter. There are two sets of polynomial expressions in the regions of $\alpha \leq 0.5$ and $\alpha \geq 0.5$. This equation can reproduce the experimental data up to the value of $kT/J \approx 0.4$. The values corresponding to minimum in the regression are $J_1 = -63.7(2)$ cm^{-1}, $J_2 = -33.4(2)$ cm^{-1} ($\alpha = 0.52$), and $g = 2.35(1)$ in the $\alpha \leq 0.5$ region. This result with $\alpha > 0.5$ indicates that the set of polynomial expressions to be used in the regression are those corresponding to $\alpha \geq 0.5$. But in the region where $\alpha \geq 0.5$ the values corresponding to the minimum in the regression are $J_1 = -49(2)$ cm^{-1}, $J_2 = -48(2)$ cm^{-1} ($\alpha = 0.97$), and $g = 2.37(1)$, which means to a practically uniform 1D $\mu_{1,3}$-azido chain with a similar J value to that obtained by using the Weng equation.[31] In fact, this was not the case because of the presence of two sets of alternating $\mu_{1,3}$-azido bridging ligands. One of them is associated with Ni–N–N angles of 116.0 and 117.0°, and a Ni–N···N–Ni torsion angle of 171.02° and the second set with Ni–N–N angles of 131.9 and 126.4°, and a Ni–N···N–Ni torsion angle of –64.3°. By taking this into consideration and the fact that the value of $\alpha = 0.52$ is very close to the upper limit of the region, we believe physically more coherent are the parameters $J_1 = -63.7(2)$ cm^{-1}, $J_2 = -33.4(2)$ cm^{-1} ($\alpha = 0.52$), and $g = 2.35(1)$ in the $\alpha \leq 0.5$ region.

The second point is the assignment of the J values of –63.7(2) and –33.4(2) cm^{-1} to the two sets of structurally different alternating $\mu_{1,3}$-azido bridging ligands. To do so, we checked the literature for magnetostructural correlations in closely related monobridged 1D *cis*-Ni-($\mu_{1,3}$-N_3)–Ni systems[1,9b,34–37] and the data are collected in Table 7. These systems have been fairly well studied and it can be concluded[1,34] that in a correlation between the $|J|$ coupling values and the structural parameters in the bridging region, the bond parameters that must be taken into account are in the order: the bond angles Ni–N–N, the Ni–N···N–Ni torsion angle, and finally the bond lengths Ni–N(azido bridging).[1,33] Maximum coupling was found for a Ni–N–N angle of 108° and decreases when Ni–N–N increases. Also, for fixed Ni–N–N angles $|J|$ is maximum for a Ni–N···N–Ni torsion angle of 180° (or 0°) and decreases when Ni–N···N–Ni increases from 0 to 90°. On the basis of this experimental finding, the highest $|J|$ value of –63.7(2) cm^{-1} calculated for compound **2** is assigned to the superexchange pathway created by the $\mu_{1,3}$-azido bridging ligands with the set of parameters Ni–N–N angles of 116.0 and 117.0°, and a Ni–N···N–Ni torsion angle of 171.02° whereas the lowest $|J|$ value of –33.4 cm^{-1} is assigned to the superexchange pathway created by the $\mu_{1,3}$-azido bridging ligands with the set of parameters Ni–N–N angles of 131.9 and 126.4°, and a Ni–N···N–Ni torsion angle of –64.3°. Also, it should be

Table 7. Structural and magnetic parameters for 1D *cis*-Ni-($\mu_{1,3}$-N_3)–Ni systems: Ni–Nα–Nβ and Ni′–Nγ–Nβ angles, τ dihedral angles [°]; J [cm^{-1}]; τ' = interplanar angle Ni–Nα···Nγ and Ni′–Nγ···Nα.

Compound[a]	Ni–N–N	Ni–N–N	τ'	τ	J	Ref.
$[Ni(3,3,3\text{-tet})_2(\mu_{1,3}\text{-}N_3)]_n(PF_6)_n$	151.8	151.3	37.2	–37.2	–18.5	[34]
$[Ni(2\text{-methyl})_2(\mu_{1,3}\text{-}N_3)]_n(ClO_4)_n$	131.8	125.9	53.9	–53.9	–16.8	[35]
$[Ni(2\text{-methyl})_2(\mu_{1,3}\text{-}N_3)]_n(PF_6)_n$	135.0	122.6	51.4	–51.4	–3.2	[35]
$[Ni(bipy)_2(\mu_{1,3}\text{-}N_3)]_n(ClO_4)_n$	123.7	120.1	46.2	133.8	–33.0	[36]
	126.6	121.3	41.0	139.0		
$[Ni(bipy)_2(\mu_{1,3}\text{-}N_3)]_n(PF_6)_n$	122.6	122.6	45.1	134.9	–22.4	[36]
	120.6	127.4	42.0	138.0		
$[Ni(aep)_2(\mu_{1,3}\text{-}N_3)]_n(ClO_4)_n$	127.8	126.2	123.4	123.4	<1	[9b]
$[Ni(abap)(\mu_{1,3}\text{-}N_3)]_n(ClO_4)_n$ (**2**)	116.0	117.0	171.0	171.0	–63.7	this work
	131.9	126.4	64.3	64.3	–33.4	
$[Ni(Me_6trien)(\mu_{1,3}\text{-}N_3)]_n(ClO_4)_n \cdot nH_2O$ (**3a**)	138.8	135.8	0.0	180	–26.8	this work
$[Ni(L)(N_3)(\mu_{1,3}\text{-}N_3)]_n$	133.4	124.5	73.2	106.8	13.5	[37]

[a] Ligand abbreviations: 3,3,3-tet = *N*,*N*′-bis(3-aminopropyl)-1,3-diaminopropane; 2-methyl = 1,2-diamino-2-methylpropane; bipy = 2,2′-bipyridyl; aep = 2-(2-aminoethyl)pyridine; abap = *N*-(2-aminoethyl)-*N*,*N*-bis(3-aminopropyl)amine; Me_6trien = 1,1,4,7,10,10-hexamethyltriethylenetetramine; L = the Schiff base of the condensation reaction of pyridine-2-carbaldehyde and *N*,*N*,2,2-tetramethylpropane-1,3-diamine.

noted that for one of the two sets of the structural parameters compound **2** reveals the highest reported $|J|$ value (Table 7). This high J value, as has been stated above, is in accordance with the nearest Ni–N–N angles to 108° and Ni–N···N–Ni torsion angle to 180°.

For compound **3a**, the χ_M value at room temperature (3.94×10^{-3} cm^3 mol^{-1}) increases as the temperature decreases, reaching a broad maximum of 9.40×10^{-3} cm^3 mol^{-1} at ca. 50 K (Figure 7). This temperature maximum clearly indicates moderate antiferromagnetic coupling between the Ni^{II} ions through the azido bridges. Below this temperature, the molar magnetic susceptibility decreases continuously and reaches a minimum value of 6.51×10^{-3} cm^3 mol^{-1} at 8 K. After this temperature, χ_M increases rapidly to a value of 11.38×10^{-3} cm^3 mol^{-1} at 2 K due to the presence of paramagnetic impurities.

Thus, taking into account that compound **3a** is structurally a uniform chain, experimental data were fitted up to near the maximum (50 K) to the Weng equation for uniform chains.[31] The best parameters so obtained were J = –26.8(1) cm^{-1} and g = 2.36(1). The J value indicates a moderate superexchange pathway. The set of parameters related with the antiferromagnetic superexchange pathway in **3a** are Ni–N–N angles of 138.8 and 135.8° and a Ni–N···N–Ni torsion angle of 180°.

Finally, it should be mentioned that the *cis* 1D Ni^{II}–azido complexes **2** and **3a** can be used as examples of low-dimensional magnetic systems to calculate the Haldane gap: for 1D systems containing integer values of the spin, S, Haldane predicted that they will exhibit a singlet ground state separated from the first triplet excited state by an energy gap E_g (Haldane gap), whereas for half-odd integer spin, this gap would not exist.[38] As a consequence in the 1D compounds at T = 0 K, χ_M has a zero value for integer spin systems and finite values for half-odd integer spin systems.[38] Thus, the integer S 1D systems with low interchain coupling are considered to be good candidates to measure the Haldane gap[39] and several well-isolated *trans* 1D azido-bridged Ni^{II} systems have been studied to demonstrate this phenomenon.[40,41] The two *cis* 1D azido-bridged Ni^{II} complexes **2** and **3a** should add further examples that potentially can serve to calculate the Haldane gap.

For the monomer compound [Ni(Me$_6$trien)(N$_3$)]ClO$_4$ (**3b**), the $\chi_M T$ vs. T plot is illustrated in Figure 8. The calculated room temperature $\chi_M T$ value of 1.29 cm^3 mol^{-1} K was found to be larger than the spin only value of 0.99 cm^3 mol^{-1} K for S = 1 in mononuclear compounds. The $\chi_M T$ value decreases slowly with decreasing temperature and at ca. 50 K the decrease is becoming too fast, reaching a $\chi_M T$ value of 0.20 cm^3 mol^{-1} K at 2 K. The experimental susceptibility data were fitted using Equation (4):[42]

$$\chi_M = (2Ng^2\beta^2/3kT)[2x^{-1} - 2\exp(-x)x^{-1} + \exp(-x)]/[1 + 2\exp(-x)] \quad (4)$$

where $x = D/kT$ and D is the Zero field splitting parameter. This equation considers only noninteracting S = 1 ions in the presence of single ion anisotropy. The best fit is given by the parameters D = 19 cm^{-1}, g = 2.22. The D value is related to the geometry around the nickel(II) ion; the high anisotropy for the pentacoordinate nickel(II) ions implies high D values.[43] The high value reported here for **3b** (19 cm^{-1}) is comparable with the high D values of 14.7 and 14.8 cm^{-1} found in similar pentacoordinate Ni^{II} compounds [Ni(Me$_5$dien)(NCS)$_2$] and [Ni(Me$_4$Etdien)(NCS)$_2$], respectively where Me$_5$dien = 1,1,4,7,7-pentamethyldiethylenetriamine and Me$_4$Etdien = 4-ethyl-1,1,7,7-tetramethyldiethylenetriamine.[43]

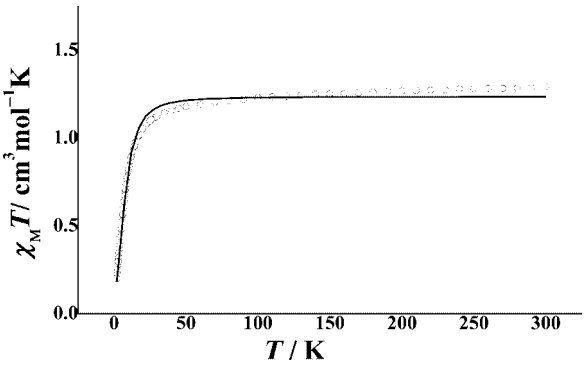

Figure 8. Plot of $\chi_M T$ vs. T in the 300–2 K temperature range for [Ni(Me$_6$trien)(N$_3$)]ClO$_4$ (**3b**) measured on cooling under an external magnetic field of 0.7 T. The solid line shows the best fit as a uniform antiferromagnetic chain (see text).

Conclusions

Bridged azido–Ni^{II} complexes have been synthesized by using tetradentate amine ligands where the Ni^{2+} centers are linked by the azido ligands in end-to-end-bond fashion. With the tripod amine trpn = N(CH$_2$CH$_2$CH$_2$NH$_2$)$_3$, dinuclear doubly bridged azido complex, [Ni$_2$(trpn)$_2$($\mu_{1,3}$-N$_3$)$_2$](ClO$_4$)$_2$ (**1**) was obtained. A small alteration in the trpn ligand skeleton to produce the corresponding tripod abap = N(CH$_2$CH$_2$CH$_2$NH$_2$)$_2$(CH$_2$CH$_2$NH$_2$), afforded the polynuclear 1D chain *cis*-[Ni(abap)($\mu_{1,3}$-N$_3$)]$_n$(ClO$_4$)$_n$ (**2**) in which the two azido groups adopt a *cis* arrangement. Surprisingly, when the tripod ligands were replaced with the linear tetradentate amine Me$_6$trien = [Me$_2$NCH$_2$CH$_2$N(Me)CH$_2$-CH$_2$N(Me)CH$_2$CH$_2$NMe$_2$], a 1D polynuclear species *cis*-[Ni(M$_6$trien)($\mu_{1,3}$-N$_3$)]$_n$(ClO$_4$)$_n$·nH$_2$O (**3a**) was also obtained with a distorted octahedral structure similar to **2**, in which the Ni–azide is extended in a zigzag chain. In complex **3a** strong steric hindrance imposed by the methyl groups of Me$_6$trien causes pronounced deviations for the two diagonal N(azide)–Ni–N(amine) bond angles from the ideal octahedral geometry. The magnetic behavior of **1**–**3a** is consistent with antiferromagnetic coupling. Compound **2** is a magnetically alternating 1D *cis* Ni($\mu_{1,3}$-N$_3$) compound, and one set of the structural parameters shows the high reported $|J|$ value. Complex **3a** is a magnetically uniform 1D *cis* Ni($\mu_{1,3}$-N$_3$) compound.

Experimental Section

Materials and Physical Measurements: 1,1,4,7,10,10-hexamethyltriethylenetetramine (Me_6trien) and *N*-(2-*b*romoethyl)phthalimide were purchased from Aldrich Chem. Co., whereas tris(3-aminopropyl)amine (trpn) was obtained from TCI-America. All other materials were reagent grade quality. Infrared spectra were recorded with a JASCO FT/IR-480 plus spectrometer as KBr pellets. Electronic spectra of the complexes in solutions were recorded with the JASCO V-550 UV/Vis. spectrophotometer and the solid spectra (diluted with $BaSO_4$) were measured by the BECKMAN DK 2A spectrophotometer using $BaSO_4$ as a standard. Elemental analyses were carried out by Atlantic Microlaboratory, Norcross, Georgia, U.S.A. Magnetic susceptibility measurements under several magnetic fields in the range 2–300 K and magnetization measurements in the field range 0.4–1 T were performed with a Quantum Design MPMS-XL SQUID magnetometer at the Magnetochemistry Service of the University of Barcelona. All measurements were performed on polycrystalline samples. Pascal's constants were used to estimate the diamagnetic corrections, which were subtracted from the experimental susceptibilities to give the corrected molar magnetic susceptibilities.

Caution: *Salts of perchlorate and azide as well as their metal complexes are potentially explosive and should be handled with great care and in small quantities.*

Synthesis of the Compounds

***N*-(2-Aminoethyl)-*N*,*N*-bis(3-aminopropyl)amine Tetrahydrochloride Trihydrate (abap·4HCl·3H_2O):** This ligand was prepared according to the literature method[44] by fusing 3,3-diphthalimidodipropylamine (observed m.p. 136–138 °C, lit. m.p. 136–137 °C) with *N*-(2-bromoethyl)phthalimide and the product, *N*-(2-phthalimidoethyl)-*N*,*N*-bis(3-phthalimidopropyl)amine, was hydrolyzed in HCl (8 M). $C_8H_{32}Cl_4N_4O_3$ (374.18): calcd. C 25.68, H 8.62, N 14.97; found C 25.54, H 8.49, N 14.55.

[Ni_2(trpn)$_2$($\mu_{1,3}$-N_3)$_2$](ClO_4)$_2$ (1): Nickel(II) perchlorate hexahydrate (0.365 g, 1.0 mmol) dissolved in H_2O (5 mL) was added to tris(3-aminopropyl)amine (0.190 g, 1.0 mmol) in H_2O (10 mL). The mixture was then heated on a steam bath for 5 min, followed by dropwise addition of an aqueous solution of NaN_3 (10 mL, 0.130 g, 2 mmol). The resulting solution was heated for another 10 min and then filtered through Celite. Slow evaporation at ambient temperature afforded mauve-blue crystals suitable for X-ray analysis. These crystals were collected by filtration, washed with cold ethanol (10 mL), ether, and air dried (yield: 0.286 g, 74%). $C_9H_{24}ClNiN_7O_4$ (388.50): calcd. C 27.82, H 6.23, N 25.24; found C 28.11, H 6.24, N 24.88. Selected IR bands (KBr): ν(N_3^-) stretching 2092 (vs); ν(Cl–O) (ClO_4^-) centered at 1092 (vs); ν(N–H) stretching at 3328 (m) and 3288 (m) cm^{-1}.

***cis*-[Ni(abap)($\mu_{1,3}$-N_3)]$_n$(ClO_4)$_n$ (2):** To abap·4HCl·3H_2O (0.372 g, 1 mmol) dissolved in H_2O (10 mL) and four equivalents of NaOH (0.160 g) was added $Ni(ClO_4)_2$·6H_2O (0.375 g, 1.0 mmol) in H_2O (10 mL). The solution was heated for 15 min and then an aqueous solution of NaN_3 (0.0720 g, 1.1 mmol in 10 mL H_2O) was added, drop by drop. The resulting blue solution was heated on a steam bath for 15 min, followed by filtration through Celite and allowed to crystallize at room temperature. After one week, the blue crystals which separated out were collected by filtration, washed with ethanol and ether and air dried (overall yield: 0.29 g, 77%). Crystals of X-ray quality were obtained from a dilute solution that was kept at room temperature. $C_8H_{22}ClNiN_7O_4$ (370.02): calcd. C 25.62, H 5.96, N 26.14; found C 25.78, H 6.00, N 26.32. Selected IR bands (KBr): ν(N_3), 2075 (vs); ν(Cl–O) (ClO_4^-), 1091 (vs); ν(N–H) stretching, 3334 (m) and 3288 (m) cm^{-1}.

[Ni(Me_6trien)(N_3)]ClO_4 (3b): The complex was prepared by a procedure similar to that described for **1** and then allowed to crystallize in the refrigerator. After two weeks, the complex was separated out as green crystals (yield: 0.348 g, 81%). Single crystals were obtained from dilute solutions. $C_{12}H_{30}ClNiN_7O_4$ (430.57): calcd. C 33.47, H 7.02, N 22.71; found C 33.48, H 7.22, N 22.77. Selected IR bands (KBr): ν(N_3^-) stretching 2060 (vs); ν(Cl–O) (ClO_4^-) 1082 (vs) cm^{-1}.

***cis*-[Ni(Me_6trien)($\mu_{1,3}$-N_3)]$_n$(ClO_4)$_n$·*n*H_2O (3a):** When the solid sample of [Ni(Me_6trien)(N_3)]ClO_4 (**3b**) was allowed to stand at room temperature for about two months, it absorbed water without losing its crystallization shape. $C_{12}H_{32}ClNiN_7O_5$ (448.59): calcd. C 32.13, H 7.19, N 21.86; found C 32.55, H 7.16, N 21.79. The IR spectrum of the hydrated sample, which was then used for single-crystal X-ray structure determination, exhibited a new band centered at 3449 cm^{-1} (mb) attributable to the ν(O–H) of lattice water and two strong bands for the azido groups at 2125 and 2092 cm^{-1}. The strong ν(Cl–O) of the perchlorate ion was detected at 1090 cm^{-1}.

Crystal Structure Analyses: The single-crystal X-ray data of compounds **1**, **2**, and **3b** were collected with a modified STOE four-circle diffractometer and that of compound **3a** with a Bruker-AXS SMART APEX CCD diffractometer. The crystallographic data, conditions retained for the intensity data collection, and some features of the structure refinements are listed in Table 8. Crystal size: 0.30 × 0.20 × 0.06 mm for **1**, 0.42 × 0.32 × 0.20 mm for **2**, 0.42 × 0.34 × 0.22 mm for **3a**, and 0.36 × 0.27 × 0.14 mm for **3b**. Intensities were collected with graphite-monochromated Mo-K_α radiation (λ = 0.7107 Å). Total of 3117 (**1**), 5926 (**2**), 3788 (**3a**), and 4069 (**3b**) reflections were nonequivalent by symmetry, and observed reflections by applying the condition $I > 2\sigma(I)$ were 2278 for **1**, 4288 for **2**, 3498 for **3a**, and 3153 for **3b**. Lorentz polarization and absorption corrections using the SADABS computer program[45] were made for **3a**, and DIFABS program[46] for **1**, **2**, and **3b**. The structures were solved by direct methods using the SHELXS-86 computer program,[47] and refined by full-matrix least-squares methods on F^2, using the SHELXL-93 program[48] incorporated in the SHELXTL/PC V 5.03 program package.[49] All non-hydrogen atoms were refined anisotropically. The hydrogen atoms were assigned with isotropic displacement factors and included in the final refinement cycles by use of geometrical restraints (C_{ar}–H = 0.93 Å; C_{Me}–H = 0.96 Å; N–H = 0.90 Å; O–H = 0.82 Å). In the case of **1**, split occupancy of 0.79(2) and 0.21(2), was applied to the disordered methylene group with atoms C(2) and C(52), respectively. In the case of **3b**, split occupancy of 0.50 was applied to atoms N(4), N(5),C(1), C(2), C(9), C(10), C(12), and C(21)–C(24) of disordered Me_6trien, respectively. The final *R* (on *F*) factors were 0.0589, 0.0572, 0.0592, and 0.0430 for the four compounds, respectively, whereas the corresponding *wR* (on F^2) were 0.1468 for **1**, 0.1504 for **2**, 0.1267 for **3a**, and 0.0986 for **3b**. Numbers of refined parameters were 210, 379, 250, and 278 for **1**, **2**, **3a**, and **3b**, respectively. Maximum and minimum peaks in the final difference Fourier syntheses were 0.556 and –0.628 e Å^{-3}, respectively, for **1**, 1.074 and –0.733 e Å^{-3}, respectively, for **2**, 0.721 and –0.593 e Å^{-3}, respectively, for **3a**, and 0.347 and –0.413 e Å^{-3}, respectively, for **3b**. The molecular plots were obtained by using the ORTEP-32 program.[50] CCDC-609516–CCDC-609518 for **1**–**3a** and CCDC-628117 for **3b** contains the supplementary crystallographic data for this paper. These data can be obtained free of charge from The Cambridge Crystallographic Data Centre via www.ccdc.cam.ac.uk/data_request/cif.

Table 8. Crystal data and structure refinement for $[Ni_2(trpn)_2(\mu_{1,3}\text{-}N_3)_2](ClO_4)_2$ (**1**), *cis*-$[Ni(abap)(\mu_{1,3}\text{-}N_3)]_n(ClO_4)_n$ (**2**), *cis*-$[Ni(Me_6trien)(\mu_{1,3}\text{-}N_3)]_n(ClO_4)_n{\cdot}nH_2O$ (**3a**), and $[Ni(Me_6trien)(N_3)]ClO_4$ (**3b**).

Compound	**1**	**2**	**3a**	**3b**
Empirical formula	$C_9H_{24}ClN_7NiO$	$C_{16}H_{44}Cl_2N_{14}Ni_2O_8$	$C_{12}H_{32}ClN_7NiO_5$	$C_{12}H_{30}ClN_7NiO_4$
Formula mass	388.49	748.93	448.59	430.57
Crystal system	monoclinic	orthorhombic	monoclinic	monoclinic
Space group	$P2_1/n$	$Pbca$	$P2_1/n$	$P2_1/n$
a [Å]	8.643(2)	12.251(4)	8.619(2)	8.723(3)
b [Å]	7.944(2)	22.144(7)	17.297(4)	15.073(4)
c [Å]	23.662(5)	22.416(7)	13.213(3)	14.569(4)
α [°]	90	90	90	90
β [°]	100.06(2)	90	90.85(3)	103.44(2)
γ [°]	90	90	90	90
V [Å^3]	1599.7(6)	6081.2(34)	1969.6(7)	1863.1(10)
Z	4	8	4	4
T [K]	100(2)	100(2)	100(2)	100(2)
μ [mm^{-1}]	1.409	1.479	1.159	1.218
$D_{calcd.}$ [Mg/m^3]	1.613	1.636	1.513	1.535
R [$I>2\sigma(I)$]	0.0589	0.0572	0.0592	0.0430
wR_2 (all data)	0.1468	0.1504	0.1267	0.0986

Acknowledgments

S. S. M. acknowledges the Summer Research Award (2005) and the financial support from the Department of Chemistry, University of Louisiana at Lafayette, and also thanks Dean B. Clark and Dr. R. B. Braun (ULL). F. A. M. thanks Prof. Kratky, Prof. Belaj (Univ. Graz), and Dr. Baumgartner (TU-Graz) for assistance.

[1] J. Ribas, A. Escuer, M. Monfort, R. Vicente, R. Cortés, L. Lezama, T. Rojo, *Coord. Chem. Rev.* **1999**, *193–195*, 1027–1068.

[2] a) M. M. Turnbull, T. Sugimoto, L. K. Thompson (Eds.), *Molecular-Based Magnetic Materials: Theory, Techniques and Applications*, ACS Symposium Series, 664, ACS, Washington, DC, **1996**; b) A. Caneschi; D. Gatteschi, L. Pardi, R. Sessoli, "Clusters, Chain and Layered Molecules: The Chemists way to Magnetic Materials" in A. F. Williams (Ed.), *Perspectives in Coordination Chemistry*, VCH, Weinheim, **1992**.

[3] a) S. S. Massoud, F. A. Mautner, *Inorg. Chim. Acta* **2005**, *358*, 3334–3340; b) A. Escuer, M. Font-Bardia, S. S. Massoud, F. A. Mautner, E. Peñalba, X. Solans, R. Vicente, *New J. Chem.* **2004**, *28*, 681–686; c) F. A. Mautner, R. Vicente, S. S. Massoud, *Polyhedron* **2006**, *25*, 1673–1680.

[4] a) A. Escuer, R. Vicente, M. S. El-Fallah, X. Solans, M. Font-Bardia, *Inorg. Chim. Acta* **1996**, *247*, 85–91; b) M. H. D'Aniello Jr, M. T. Mocella, F. Wagner, E. K. Barefield, I. C. Paul, *J. Am. Chem. Soc.* **1975**, *97*, 192–194; c) D. Sellmann, R. Prakash, F. Geipel, F. W. Heinemann, *Eur. J. Inorg. Chem.* **2002**, 2138–2146; d) N. Mondal, S. Mitra, V. Gramilich, S. K. Ghodsi, K. M. A. Malik, *Polyhedron* **2001**, *20*, 135–141; e) J.-P. Costes, F. Dahan, J. M. Dominguez-Vera, J.-P. Laurent, J. Ruiz, J. Sotiropoulos, *Inorg. Chem.* **1994**, *33*, 3908–3913.

[5] a) A. J. Blake, F. A. Devillanova, A. Garau, A. Harrison, F. Isaia, V. Lippolis, S. K. Tiwary, M. Schroder, G. Verani, G. Whittaker, *J. Chem. Soc., Dalton Trans.* **2002**, 4389–4394; b) A. McAuley, D. G. Fortier, D. H. Macartney, T. W. Whitcombe, C. Xu, *J. Chem. Soc., Dalton Trans.* **1994**, 2071–2079; c) C. Dietz, F. W. Heinemann, J. Kuhnigk, C. Kruger, M. Gerdan, A. X. Trautwein, A. Grohmann, *Eur. J. Inorg. Chem.* **1998**, 1041–1049.

[6] a) L. Li, D. Liao, Z. Jiang, S. Yin, *J. Mol. Struct.* **2003**, *649*, 37–42; b) K.-Y. Choi, K.-M. Chun, K.-C. Lee, J. Kim, *Polyhedron* **2002**, *21*, 1913–1920; c) K.-Y. Choi, H. Ryu, I.-H. Suh, *Polyhedron* **1998**, *17*, 1241–1246; d) M. K. Urtiaga, M. I. Arriortua, I. G. De Muro, R. Cortés, *Acta Crystallogr., Sect. C: Cryst. Struct. Commun.* **1995**, *51*, 62–65.

[7] M. Monfort, I. Resino, J. Ribas, X. Solans, M. Font-Bardia, H. Stoeckli-Evans, *New J. Chem.* **2002**, *26*, 1601–1606.

[8] J. Hausmann, M. H. Klingele, V. Lozan, G. Steinfeld, D. Siebert, Y. Journaux, J. J. Girerd, B. Kersting, *Chem. Eur. J.* **2004**, *10*, 1716–1728.

[9] a) J. Ribas, M. Monfort, C. Diaz, C. Bastos, X. Solans, *Inorg. Chem.* **1993**, *32*, 3557–3561; b) J. Ribas, M. Monfort, B. K. Ghosh, R. Cortés, X. Solans, M. Font-Bardia, *Inorg. Chem.* **1996**, *35*, 864–868.

[10] F. Fabrizi de Biani, E. Ruiz, J. Cano, J. J. Novoa, S. Alvarez, *Inorg. Chem.* **2000**, *39*, 3221–3229.

[11] B. Kersting, G. Steinfeld, D. Siebert, *Chem. Eur. J.* **2001**, *7*, 4253–4258.

[12] C. G. Pierpont, D. N. Hendrickson, D. M. Duggan, F. Wagner, E. K. Barefield, *Inorg. Chem.* **1975**, *14*, 604–610.

[13] P. Chaudhuri, M. Guttmann, D. Ventur, K. Wieghardt, B. Nuber, J. Weiss, *J. Chem. Soc., Chem. Commun.* **1985**, 1618–1620.

[14] Q.-L. Wang, X.-Q. Jia, D.-Z. Liao, S.-P. Yan, P. Cheng, G.-M. Yang, H.-X. Ren, Z.-H. Jiang, *Transition Met. Chem.* **2006**, *31*, 434–440.

[15] C. S. Hong, Y. Do, *Angew. Chem. Int. Ed.* **1999**, *38*, 193–195.

[16] R. Vicente, A. Escuer, J. Ribas, M. S. El-Fallah, X. Solans, M. Font-Bardia, *Inorg. Chem.* **1993**, *32*, 1920–1924.

[17] a) S. Sarkar, A. Mondal, M. S. El-Fallah, J. Ribas, D. Chopra, H. Stoeckli-Evans, K. K. Rajak, *Polyhedron* **2006**, *25*, 25–30; b) S. Deoghoria, S. Sain, M. Soler, W. T. Wong, G. Christou, S. K. Bera, S. K. Chandra, *Polyhedron* **2003**, *22*, 257–262; c) X.-J. Liu, Z. Shen, Y. Song, H.-J. Xu, Y.-Z. Li, X.-Z. You, *Inorg. Chim. Acta* **2005**, *358*, 1963–1969.

[18] G. Leibeling, S. Demeshko, B. Bauer-Siebenlist, F. Meyer, H. Pritzkow, *Eur. J. Inorg. Chem.* **2004**, 2413–2420.

[19] F. Meyer, P. Kircher, H. Pritzkow, *Chem. Commun.* **2003**, 774–775.

[20] F. Meyer, S. Demeshko, G. Leibeling, B. Keresting, E. Kaifer, H. Pritzkow, *Chem. Eur. J.* **2005**, *11*, 1518–1526.

[21] a) S. Demeshko, G. Leibeling, W. Maringgele, F. Meyer, C. Mennerich, H.-H. Klauss, H. Pritzkow, *Inorg. Chem.* **2005**, *44*, 519–528; b) T. K. Karmakar, S. K. Chandra, J. Ribas, G. Mostafa, T. H. Lu, B. K. Ghosh, *Chem. Commun.* **2002**, 2364–2365.

[22] a) J. Ribas, M. Monfort, B. K. Ghosh, R. Cortés, X. Solans, M. Font-Bardia, *Inorg. Chem.* **1996**, *35*, 864–868; b) M. Monfort, J. Ribas, X. Solans, M. Font-Bardia, *Inorg. Chem.* **1996**, *35*, 7633–7638.

[23] M. S. El-Fallah, A. Escuer, R. Vicente, X. Solans, M. Font-Bardia, M. Verdaguer, *Inorg. Chim. Acta* **2003**, *344*, 133–142.

[24] M. A. S. Goher, A. Escuer, F. A. Mautner, N. A. Al-Salem, *Polyhedron* **2002**, *21*, 1871–1876.

[25] a) A. Escuer, R. Vicente, M. S. El-Fallah, S. B. Kumar, F. A. Mautner, D. Gatteschi, *J. Chem. Soc., Dalton Trans.* **1998**, 3905–3909; b) R. Vicente, A. Escuer, *Polyhedron* **1995**, *14*, 2133–2138; c) R. Vicente, A. Escuer, J. Ribas, X. Solans, *Inorg. Chem.* **1992**, *31*, 1726–1728; d) F. Meyer, H. Pritzkow, *Inorg. Chem. Commun.* **2001**, *4*, 305–307.

[26] a) M. Monfort, I. Resino, J. Ribas, X. Solans, M. Font-Bardia, *New J. Chem.* **2001**, *25*, 1577–1582; b) M. Monfort, I. Resino, X. Solans, M. Font-Bardia, P. Rabu, M. Drillon, *Inorg. Chem.* **2000**, *39*, 2572–2576; c) L. Li, D. Liao, Z. Jiang, S. Yan, *Polyhedron* **2000**, *19*, 1575–1578; d) P. Chaudhuri, T. Weyhermuller, E. Bill, K. Wieghardt, *Inorg. Chim. Acta* **1996**, *252*, 195–202.

[27] a) M. Monfort, I. Resino, J. Ribas, H. Stoeckli-Evans, *Angew. Chem. Int. Ed.* **2000**, *39*, 191–193; b) M. L. Hernández, M. G. Barandika, M. K. Urtiaga, R. Cortés, L. Lezama, M. I. Arriortua, *J. Chem. Soc., Dalton Trans.* **2000**, 79–84.

[28] a) A. Escuer, R. Vicente, F. A. Mautner, M. A. S. Goher, M. A. M. Abu-Youssef, *Chem. Commun.* **2002**, 64–65; b) F. A. Mautner, R. Cortés, L. Lezama, T. Rojo, *Angew. Chem. Int. Ed. Engl.* **1996**, *35*, 78–80.

[29] A. W. Addison, T. N. Rao, J. Reedijk, J. van Rijn, G. C. Verschoor, *J. Chem. Soc., Dalton Trans.* **1984**, 1349–1356.

[30] a) A. P. B. Lever, *Inorganic Electronic Spectroscopy*, Elsevier, Amsterdam, **1984**, pp. 513–520; b) M. D. Santana, G. Garcia, M. Julve, F. Lloret, J. Pérez, M. Liu, F. Sanz, J. Cano, G. López, *Inorg. Chem.* **2004**, *43*, 2132–2140; c) M. D. Santana, A. A. Lozano, G. Garcia, G. López, J. Pérez, *Dalton Trans.* **2005**, 104–109.

[31] C. Y. Weng, Ph. D. Thesis, Carnegie Institute of Technology, **1968**.

[32] a) A. Escuer, R. Vicente, J. Ribas, M. S. El Fallah, X. Solans, *Inorg. Chem.* **1993**, *32*, 1033–1035; b) A. Escuer, R. Vicente, J. Ribas, M. S. El Fallah, X. Solans, M. Font-Bardía, *Inorg. Chem.* **1993**, *32*, 3727–3732.

[33] J. J. Borrás Almenar, E. Coronado, J. Curely, R. Georges, *Inorg. Chem.* **1995**, *34*, 2699–2704.

[34] A. Escuer, R. Vicente, J. Ribas, M. S. El-Fallah, X. Solans, M. Font-Bardía, *Inorg. Chem.* **1994**, *33*, 1842–1847.

[35] J. Ribas, M. Monfort, C. Diaz, C. Bastos, C. Mer, X. Solans, *Inorg. Chem.* **1995**, *34*, 4986–4990.

[36] R. Cortes, K. Urtiaga, L. Lezama, J. L. Pizarro, A. Goñi, M. I. Arriortua, T. Rojo, *Inorg. Chem.* **1994**, *33*, 4009–4015.

[37] P. S. Mukherjee, S. Dalai, E. Zangrando, F. Lloret, N. R. Chaudhuri, *Chem. Commun.* **2001**, 1444–1445.

[38] a) F. D. Haldane, *Phys. Lett.* **1983**, *93A*, 464–468; b) J. P. Renard, M. Verdaguer, L. P. Regnault, W. A. K. Erkelens, J. Rossat-Mignod, W. G. Stirling, *Europhys. Lett.* **1987**, *3*, 945–952; c) I. Affleck, T. Kennedy, E. H. Lieb, H. Tasaki, *Phys. Rev. Lett.* **1987**, *59*, 799–802.

[39] a) T. Ishii, N. Aizawa, H. Hara, M. Yamashita, H. Matsuzaka, *Polyhedron* **2001**, *20*, 1297–1304; b) T. Takeuchi, M. Ono, H. Hori, T. Yosida, A. Yamagishi, M. Date, *J. Phys. Soc. Jpn.* **1992**, *61*, 3255–3261.

[40] a) M. S. El Fallah, A. Escuer, R. Vicente, X. Solans, M. Font-Bardia, M. Verdaguer, *Inorg. Chim. Acta* **2003**, *344*, 133–142; b) M. Kohno, M. Takahashi, M. Hagiwara, *Phys. Rev. B* **1998**, *57*, 1046–1051; c) L. K. Chou, D. R. Talham, W. W. Kim, P.-J. C. Signore, M. W. Meisel, *Physica B* **1994**, *194*, 313–314; d) T. Takeuchi, H. Hori, M. Date, T. Yosida, K. Katsumata, J. P. Renard, V. Gadet, M. Verdaguer, *J. Magn. Magn. Mater.* **1992**, *194*, 813–814.

[41] a) T. Manabe, M. Yamashita, T. Ohishi, T. Takeuchi, T. Yosida, Y. Yu, Z. Honda, K. Katsumata, *Synth. Met.* **1997**, *85*, 1717–1718; b) M. Yamashita, K. Inoue, T. Ohishi, H. Miyamae, T. Takeuchi, T. Yosida, *Synth. Met.* **1995**, *71*, 1961–1964.

[42] C. P. Landee, D. M. Mudgett, B. M. Foxman, *Inorg. Chim. Acta* **1991**, *186*, 45–49.

[43] R. Vicente, A. Escuer, X. Solans, M. Font-Bardía, *Inorg. Chim. Acta* **1996**, *248*, 59–65.

[44] a) R. L. Fanshawe, A. G. Blackman, *Inorg. Chem.* **1995**, *34*, 421–423; b) R. L. Fanshawe, A. G. Blackman, C. R. Clark, *Inorg. Chim. Acta* **2003**, *342*, 114–124.

[45] R. H. Blessing, *Acta Crystallogr. Sect. A* **1995**, *51*, 33–38; SADABS, Bruker AXS, **1998**.

[46] N. Walker, D. Stuart, *Acta Crystallogr., Sect. A* **1983**, *39*, 158–166.

[47] G. M. Sheldrick, *SHELXS-86, Program for the solution of crystal structures*, University of Göttingen, Göttingen, Germany, **1986**.

[48] G. M. Sheldrick, *SHELXL-93, Program for the refinement of crystal structures*, University of Göttingen, Göttingen, Germany, **1993**.

[49] *SHELXTL 5.03 (PC-Version), Program library for the solution and molecular graphics*, Siemens Analytical Instruments Division, Madison, WI, **1995**.

[50] *ORTEP-32 for Windows*: L. J. Farrugia, *J. Appl. Crystallogr.* **1997**, *30*, 565.

Received: August 3, 2006
Published Online: February 9, 2007

